A Coupled Thermo - Mechanical Model for Deformation in High Temperature-Low Pressure Metamorphic Terrains:implications for the Palmer region, Southern Adelaide Fold Belt.

by

Nicholas Martin

Submitted as partial fulfilment for the Honours degree of Bachelor of Science.

Department of Geology and Geophysics
University of Adelaide
November, 1990

Contents.

Abstract

Peak metamorphic growth in high temperature - low pressure terrains is commonly associated with crustal thickening strains reflected in syn - tectonic fabrics. Conductive heat transfer through the lithosphere for geologically plausible thermal and mechanical configurations is unable to produce such temperatures and thus an advective thermal perturbation is required, and is commonly in the form of granitic melts. Thermal weakening of the lithosphere as a consequence of this advective heat allows the potential for crustal thickening strain increments. In this thesis a coupled thermo - mechanical model is presented which allows quantification of this thermal weakening effect. Two granite generation models are investigated; firstly, lower crustal melting due to conductive heating of the lithosphere during orogenesis and secondly, segregation or roof rock melting from mafic sills located at the base of the crust. Results from the model indicate that, for granites produced by melting of the lower crust, crustal thickening strains increments are only in the order of 5 -10 %. However, for granites produced by segregation from a mafic sill crustal strain increments of up to 30% may occur during emplacement. Thus in order to produce peak metamorphic temperatures associated with significant crustal strain a system analogous to the second model is required. Structural and metamorphic studies of the Palmer region in the Southern Adelaide Fold Belt reveal the associated development of partial melting and peak metamorphism with the intrusion of the orthogneissic Rathjen Gneiss during the regional D_1 folding event. Thermal weakening triggered by the Rathjen Gneiss has produced a local D_2 folding event. Areas at some distance from the Rathjen Gneiss exhibit peak metamorphic growth during D_2 consistant with the delayed peak temperatures from the cooling body.

1. INTRODUCTION

High temperature-low pressure (high T - low P) metamorphic terrains are commonly characterized by prograde mineral fabrics indicating peak metamorphism during crustal thickening (Gans and Miller,1989). Simple thermal considerations have shown that for reasonable convergent deformation geometries the maximum achievable temperatures by conductive heat transfer alone at depths appropriate to low pressure terrains is only in the order of 500°C (Sandiford and Powell 1990, in press). Consequently an additional heat source is required to generate high temperature-low pressure terrains. Loosveld (1989), Loosveld and Etheridge (1990) and Sandiford (1989) have shown that the response of the lower lithosphere during convergent deformation is critical to raising the mantle heat flux during orogenesis. This increase in the mantle heat flux will result in an increase in temperatures throughout the crust eventually allowing the potential for melting at the base of the crust and granite generation. Diapiric rise of the silicic magmas may make significant contributions to mid crustal thermal perturbation. Such magmatic intrusion must have important local mechanical consequences for the orogenic event (eg. Gans and Miller, 1989) because of the lithospheric strength dependence on temperature (Ord and Hobbs, 1990). Figure 1 shows schematically that during deformation the intrusion of a magmatic body will cause local heating and weakening of the surrounding country rock resulting in small increments in homogeneous crustal thickening strains.

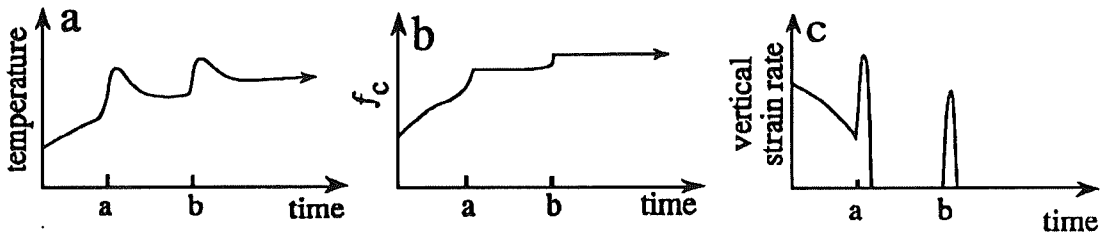

Figure 1.

Figure 1a shows schematically the effects of thermal perturbation on the temperature evolution of a deforming orogen. These thermal perturbations will result in local decreases in lithospheric strength and consequentially increases in crustal strain increments, f_c (Fig.1b) with rapid increases in vertical strain rates. Synchronous timing of peak temperatures and high strain rates will allow mineral growth during crustal thickening and the development of syn-tectonic fabrics. (after Sandiford and Powell, in press)

In this thesis a coupled thermo-mechanical numerical model is used in order to constrain the mechanical effects of an advective thermal pulse on the regional deformation in an orogenic belt. A field study of the Kanmantoo Group, in the Palmer region, and related igneous intrusives, the Rathjen Gneiss and the Palmer Granite, is incorporated in order to investigate the field relationships between syn-tectonic magmatic intrusion and the deformation and metamorphism in a low pressure 'Buchan style' metamorphic terrain.

2. MODEL FORMULATION

The basic aim of this model is to quantify the mechanical response of the lithosphere to the introduction of advective heat via granitic emplacement in the upper lithosphere and the consequent changes in the potential for regional deformation. The lithosphere is modelled in one dimension (depth) since length scales for continental orogenesis are far greater than the thickness of the lithosphere. This section outlines the assumptions and the physical basis for the numerical model giving the governing equations for the thermal and mechanical evolution for the lithosphere and assumed rheological properties. This model uses a thermal model for magmatic heat developed separately (see Fraser, 1990). The mathematical derivations for the governing equations are derived in appendix A.

2.1. Rheology

The response of the lithosphere to an applied force depends on its material properties and thermal structure. The choices for mineralogical composition in the lithosphere is critical because of the significant variation in the strength of minerals. Experimental work by Shelton and Tullis (1981) has shown that the strength of a poly-phase rock can be approximated by a single strength controlling mineral phase provided that it forms more than 30% of the rock. For rocks with more than one phase in proportions above 30% the strength of the rock is governed by the weaker of the minerals. In the model presented here the lithosphere will be simply treated as a quartz dominated crust and olivine dominated mantle lithosphere following the work of Brace and Kohlstedt (1980). Table 1 shows the experimentally derived material properties used for the individual layers.

Symbol		Value/units
ρ_c	crustal density	2750 kg m^{-3}
ρ_m	mantle density	3300 kg m^{-3}
A_q	pre-exponential const. for quartz flow	5×10^{-6} MPa^{-3}
A_o	pre-exponential const. for olivine flow	7×10^{4} MPa^{-3}
Q_q	activation energy for quartz flow	1.5×10^{5} J mol^{-1}
Q_o	activation energy for olivine flow	5.2×10^{5} J mol^{-1}
n	stress exponential	3
R	Gas constant	8.3144 J K^{-1}
g	gravitational acceleration	9.8 ms^{-2}
μ_1	coeff. of frictional sliding	0.85 (<200 MPa)
μ_2	coeff. of frictional sliding	0.6 (<200 MPa)
c_1	constant < 200 MPa	0
c_2	constant > 200 MPa	60

Table 1

Material properties used in equations (1) and (2).

In order to investigate the thermal and mechanical consequences of deformation it is necessary to apply a constitutive equation that relates stress to the strain rate and temperature. In the upper regions of the crust under conditions of low temperatures and confining pressures the lithosphere will undergo brittle deformation (thrust faulting in convergent deformation). Failure under these conditions will be by frictional sliding and is commonly ascribed to obey a form of Byrelee's law (Byrlee, 1968):

$$\sigma_1 - \sigma_3 = c + \mu \rho g z \qquad (1)$$

where $\sigma_1 - \sigma_3$ is deviatoric stress, μ is the internal frictional constant, g is the acceleration due to gravity, ρ is density and z is depth.

At higher confining pressure and temperatures the rocks will reach a critical depth at which they will yield preferentially by ductile deformation at lower shear stresses than equation (1) with the change in the mode of failure corresponding to the brittle-ductile transition. Ductile deformation can be described by a temperature and strain rate dependent power creep law of the form (eg.. Goetze, 1978):

$$\sigma_1 - \sigma_3 = \left(\frac{\dot{\varepsilon}}{A}\right)^{1/n} \exp(Q/nRT) \qquad (2)$$

where $\dot{\varepsilon}$ is strain rate, A a material constant, n is a power law exponent, Q is the activation energy, R the gas constant and T the temperature.

Figure 2 shows schematically the strength verses depth curve for the quartz dominated crust and the olivine dominated mantle lithosphere (bold line). Under conditions of sufficiently low geothermal gradient and high strain rate the upper portion of the mantle lithosphere may undergo failure by frictional sliding. In the ductile failure regime it is shown that the strength is exponentially dependent on the temperature and consequentially depth with little or no effective strength at the base of the crust and lithosphere.

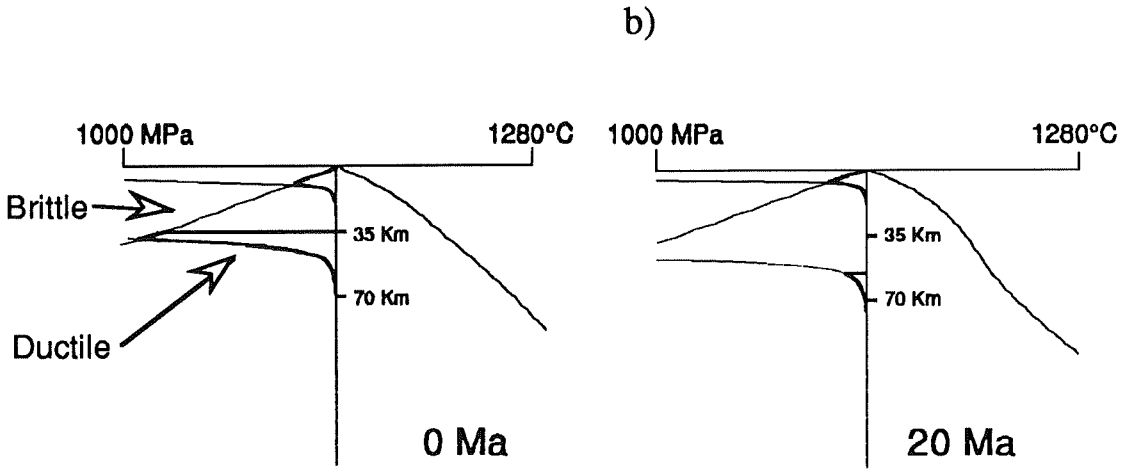

Figure 2.

The strength curve (in bold) indicates that at any depth the lithosphere will yield preferentially by the lower shear stress between brittle and ductile failure curves. Fig. 2a shows that at lower levels under conditions of low confining pressure and temperature brittle failure via frictional sliding will occur. This will give way to ductile deformation at higher temperatures and pressures with strength decaying exponentially with depth. Fig 2b shows that after temperature increases as a consequence of crustal thickening and orogenic heating there is a dramatic decline in the maximum sustainable shear stress of the upper lithosphere in comparison to only a minor decrease in the crust.

The shear strength of the lithosphere per unit length of the orogen, F_S, is given by integration of the strength profile with respect to depth:

$$F_S = \int_0^{zl} (\sigma_1 - \sigma_3)\, dz \qquad (3)$$

where zl is the depth to the base of the lithosphere.

It is important to note that these experimental data must be used with some caution as discussed in detail by Patterson (1987), as the experimental methods are conducted at strain rates greater than $\times 10^5$ s^{-1} that of natural strain rates and thus create the potential for considerable error.

2.2. Mechanical considerations

Deformation of the continental lithosphere is the result of plate tectonic convergence or extension which is driven by oceanic plate subduction and mid-ocean ridge push. The magnitudes for these forces are in the order of 3×10^{13} Nm^{-1} and $4 \times 10^{12} Nm^{-1}$ respectively (Turcotte and Schubert, 1982) and provide a plausible range for continental orogenesis. The driving force, F_{dc}, for deformation in this numerical model will be kept at a constant throughout the orogenic event. Compressional driving forces will result in plane strain horizontal shortening and vertical stretching of the lithosphere. The deformation must therefore give rise to topographic contrasts at the boundaries between the deformed and reference non-deformed lithosphere. These topographic contrasts will give rise to significant vertical stress gradients resulting in buoyancy forces, F_b (Turcotte and Schubert, 1982). The buoyancy force can be approximated by the vertically integrated vertical stress difference between the deformed and reference undeformed lithosphere:

$$F_b = \int_{zl}^{h_o} \sigma_{zzo}(z)\, dz \; - \int_{zl}^{h_o+h} \sigma_{zzd}(z)\, dz \qquad (4)$$

where h_o is the initial surface elevation, h is the elevation due to deformation, σ_{zzo} and σ_{zzd} are the vertical averaged stresses for the non-deformed and deformed lithosphere respectively. Equation (4) may be approximated in terms of crustal thickening strain, f_c, and lithospheric thickening strain, f_l, after Sandiford and Powell (1990) (appendix A). As buoyancy forces increase during orogenesis an increasing proportion of the driving force will be partitioned to

supporting the topographic elevation thus decreasing the effective driving force causing the deformation. This effective driving force, F_{edc}, can be expressed as a simple force balance of the form:

$$F_{edc} = F_{dc} - F_b = F_s \quad (5)$$

Thus the theoretical limit to deformation is when the buoyancy force is equivalent to the driving force with the effective driving force and strength decreased to zero.

2.3. Role of the Lower Lithosphere

Topographic and density gradients, discussed above, are not restricted to the surface but will also occur at the Moho and the base of the lithosphere. Theoretical modelling by Houseman *et al* (1981) have shown that the displacement of cold lithospheric material down into hot asthenosphere may result in the gravitational instability of the lower lithosphere with the potential for convective stripping of this mantle portion of the lithosphere. This may have a dramatic effect on the thermal structure of the lithosphere (Houseman *et al* , 1981) and may be responsible for melting and granite generation. In addition to this process the upwelling of hot, buoyant asthenospheric material will create considerable potential energy (England and Houseman, 1988). In this investigation two hypothetical mantle lithosphere responses will be modelled in comparison to a model of homogeneous thickening of the both the crustal and mantle part of the lithosphere.

i) constant mantle heat flow across the Moho (strain model 1; appendix C). This strain model approximates a thermally stabilized lithosphere, that is the heat fluxes in and out of the orogen remain a constant. As a consequence of this the thermal gradient in the mantle lithosphere will remain a constant and in order to preserve this during conductive heating thinning of the mantle lithosphere must occur.

ii) constant thickness of the mantle portion of the lithosphere (strain model 2; appendix C). The heat flow across the Moho will then decrease with time as the thickness of the mantle is increasing relative to strain model 1

2.4. Thermal considerations

The principal mode of heat transfer through the lithosphere is by conduction. The steady state thermal structure of the lithosphere can be derived from a simple thermal energy balance (appendix A). Measured values for the surface heat flux, q_s, range from 45mWm^{-2} to 120 mWm^{-2} near granitic provinces with an average of 65-75 mWm^{-2} in modern continental crust (Turcotte and Schubert, 1982). Typical mantle heat flux at the Moho are in the order of only 30 mWm^{-2} (Turcotte and Schubert, 1982) with the remainder of the surface heat flow made up by internal radiogenic heat producing elements. The vertical distribution of these radiogenic elements is poorly understood and has been assumed here to be restricted to the crust where it is homogeneously distributed and appropriate for thrust terrains (England and Thompson, 1984). Initially the lithosphere has been assumed to be in steady state (ie. the change in temperature with respect to time is zero) .

$$\frac{\partial T}{\partial t} = 0 = K\frac{\partial^2 T}{\partial z^2} + H \qquad (6)$$

where t is time, T is temperature, H is the heat production (Wm^{-3}) and K is conductivity.

During deformation however, the lithosphere will no longer be in steady state and the gain in thermal energy during deformation can be described by a diffusion - advection equation which has been solved by a Crank-Nicolson finite difference approximation:

$$\frac{\partial T}{\partial t} = \kappa\frac{\partial^2 T}{\partial z^2} - \upsilon\frac{\partial T}{\partial z} + \frac{H}{\rho\, c_p} \qquad (7)$$

where υ is vertical velocity, c_p is heat capacity, κ is diffusivity and H is heat production. The second term on the right hand side is the advective derivative and describes the change in temperature with respect to time due to movement of the lithosphere through a spatially varying temperature field (Turcotte and Schubert, 1982). Coupled with Eqn. (7) in this model is the introduction of advective heat in the form of magmatic intrusion. The investigations here have been done in conjunction with the thermal modeling of an intrusion by Fraser (1990) which examines the thermal consequences of a cooling magmatic sill. Two models for the generation of magmas will be investigated here. Firstly, magmas produced by the lower crustal melting as

a result of the lower crust reaching a critical melting temperaturerange of 750 - 800° C due to conductive heating. Secondly underplating of mafic magma at the base of the crust with segregation or roof rock melting of silicic melts due to thermal interaction between the mafic sill and lower crust.

3. RESULTS and DISCUSSION

The results of the modeling are shown in figure 3-5 where they are in four forms: buoyancy force to driving force ratio (F_b'), crustal thickening strain (f_c), strain rate and crustal strength to lithospheric strength ratio (F_c') with each being shown as a function of time. Each model has been run for three different initial thermal configurations namely surface heat fluxes of 80, 85 and 90 mWm^{-2} respectively. These high heat fluxes are well in excess of those experienced by any stable continental lithosphere but are appropriate to rifted or magmatic tectonic settings.

Figures 3 and 4 show the results for which silicic magmas are the product of lower crustal melting alone. Heating of the lithosphere is due primarily to the increase in the radiogenic producing elements as the heat flux across the Moho, q_m, remains either a constant or decreases slightly for strain models 1 and 2 respectively during orogenesis. This increase in internal heat production will elevate temperatures at the base of the crust to 750°- 800°C at which the lower crust may undergo melting and the production of silicic melts. Figure 3a shows the dependence on timing of this melting for each thermal configuration. Surface heat fluxes of 90 mWm^{-2} or more will result in a hotter geothermal gradient (appendix B) with temperatures at the Moho in excess of 600°C. Thus only a short time span, 20 - 30 Ma, is required to elevate temperatures in the lower crust to that of the critical 750 - 800° C range for melting. In contrast the runs with a low lithospheric surface heat flux (80 mWm^{-2} or less) and consequently a cooler geothermal gradient, a greater amount of crustal thickening, and consequently time (over 70 Ma), will be required for generation of the temperatures required for magma formation at the base of the crust. Lowering of the mantle heat flux with time, as seen in model 2 (Fig. 3e), means temperatures in the lower crust will not reach melting temperatures until well over 100 Ma after the onset of orogenesis.

Due to the relative low density of the silicic magmas in comparison to the lithosphere they will buoyantly ascend to the lower levels of the crust with the level of emplacement of these magmas controlled predominantly by the shear strength of the lithosphere, assuming no temperature or viscosity changes during ascent. At the site of generation of the magmas much of the shear strength of the lithosphere is concentrated in the upper crust and thus the rising magma will encounter little resistance (Fig. 2b). However, shear strength will increase at shallower depths until it reaches the same magnitude as the buoyancy force of the magma, effectively trapping the pluton at that level. This depth is consistently 10-15 km and becomes critical to the effect on the strain in the lithosphere as will be discussed later. Figures 3d and 3h show that at the time of lower crustal melting, for each thermal configuration, and magma emplacement there is little shear strength in the lower crust and mantle lithosphere with buoyancy forces approaching the same magnitude as the driving forces (Figs. 3c and 3g). Rapid thermal weakening will quickly lower the strength of the lithosphere to near zero increasing the vertical crustal strain increments with buoyancy force approaching the same magnitude as driving force and thus the effective driving force will tend to zero, halting deformation (Eqn. 5). These increases in crustal strain increments are in the order of 5-10% of the total crustal strain before the limiting condition for deformation is reached and last only in the order of 2-3 Ma (Figs 3c and 3g). This minor amount of crustal thickening strain as compared to the total for the orogenic event is unlikely to produce significant regional deformation with penetrative syn - tectonic fabrics . Figures 4 illustrates the importance of thickness and level of emplacement on the crustal strain and time scales involved. Increasing the thickness from 1.1 km to 4.4 km (Fig. 4a-b and 4c-d) increases the amount of associated crustal strain with correspondingly higher strain rates however, the crustal thickening strain in both cases still only forms a minor portion of the total crustal thickening strain. Emplacement levels of approximately 10 km (Fig. 4a-c) correspond to the approximate depth of the brittle - ductile transition and a majority of the crustal strength (Fig. 2b). Thus the introduction of a thermal perturbation will allow the potential for rapid decreases in crustal strength and consequentially increases in buoyancy force. However, at lower levels of intrusion (15 km, Fig. 4e and 4f) higher ambient temperatures associated with comparatively

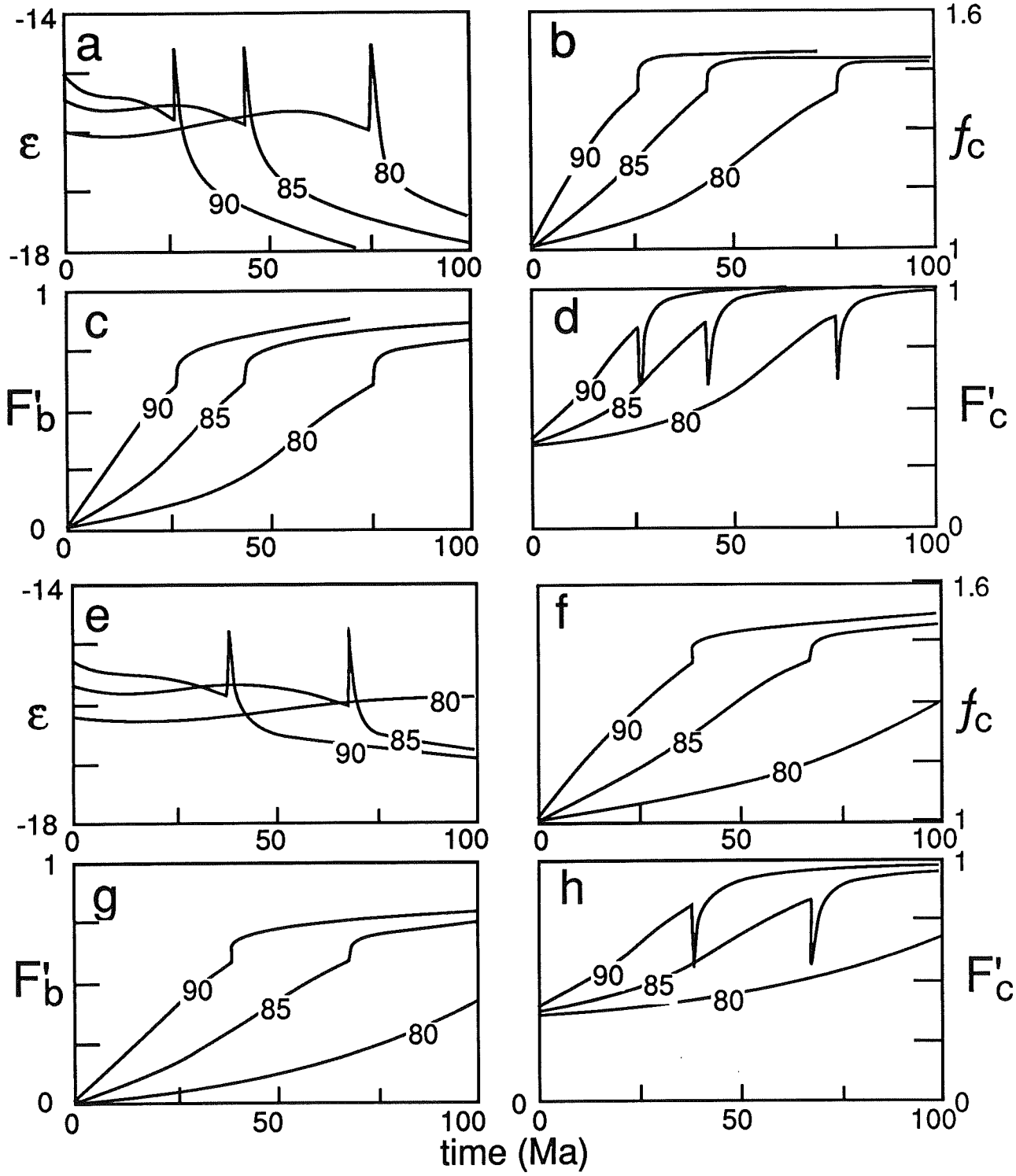

Figure 3

Plots for log strain rate, $\dot{\varepsilon}$, crustal thickening factor, f_c, buoyancy force on driving force, $F_b' = F_b/F_{dc}$ and crustal strength on lithospheric strength, $F_c' = F_{sc}/F_{sl}$, all against time. Figures 3a- d correspond to strain model 1 with a driving force of 5×10^{12} Nm^{-1}, intrusion top at 10.2 km with a granite thickness of 2.3 km. Figures 3e- h correspond to strain model 2 with a driving force of 4.5×10^{12} Nm^{-1}, intrusion top at 9.8 km with a granite thickness of 2.2 km. Each model has been run for surface heat fluxes of 80, 85 and 90 mWm^{-2}

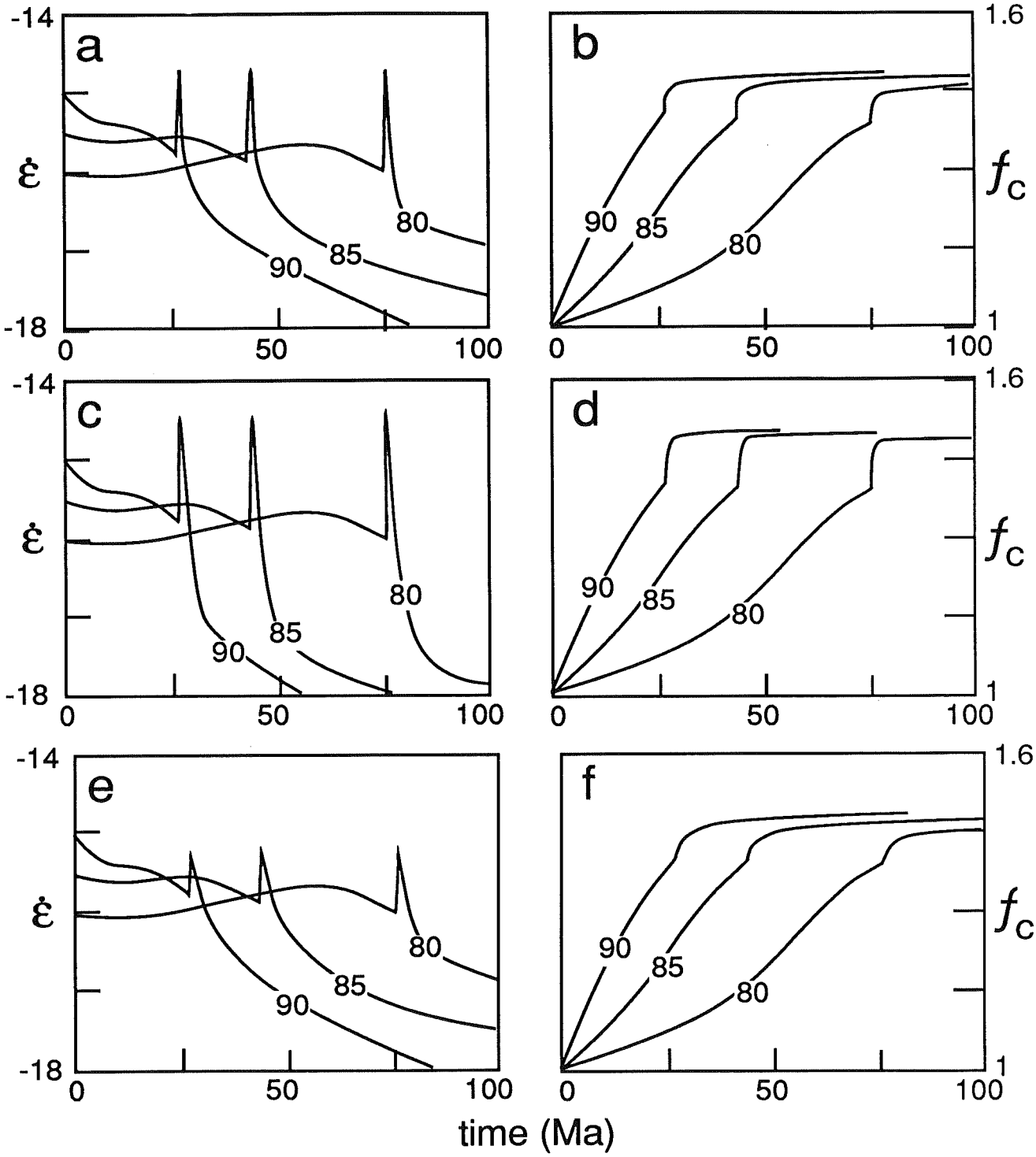

Figure 4

Figure 4 illustrates the dependence of depth and thickness on the mechanical response of the lithosphere. Plots are for log strain rate, $\dot{\varepsilon}$ and crustal thickening factor, f_c, against time. All plots are for strain model 1 and therefore a driving force of 5×10^{12} N/m. Figures 4a and 4b corresponding intrusion top at 10.2 km with a granite thickness of 1.1 km. Figures 4c and 4d corresponding intrusion top at 10.2 km with a granite thickness of 4.4 km. Figures 4e and 4f corresponding intrusion top at 15.2 km with a granite thickness of 2.2 km. Each model has been run for surface heat fluxes of 80, 85 and 90 mWm^{-2}.

minor crustal strength will dampen the thermal effects of the magma with only the potential for minor crustal thickening strain.

In contrast to the above model, segregation or roof rock melting of a mafic sill to produce silicic magma has the potential for significant crustal strain increments. Decompression or mantle plumes will cause local generation of mafic magmas in the lower mantle and the asthenosphere. These melts will rise diapirically, however, this ascent is likely to be terminated by the density contrast at the Moho resulting in the concentration of these mafic magmas in the lower crust and at the Moho discontinuity. Thermal exchange between the mafic magma and the lower crust will allow the potential for significant intermediate to silicic magma generation. Fluid dynamic studies on the roof interactions between a mafic sill and the lower crust have been conducted by Huppert and Sparks (1988). Their results suggest that the amount of silicic magma produced is approximately half that of the original thickness of the resultant mafic sill with the time scales for generation much shorter ($\times 10^{2}$yrs) compared to the life span of the silicic magma system ($\times 10^{7\text{-}8}$yrs). Thus emplacement of both the mafic sill at the base of the crust and production of silicic magma in the upper crust can be approximated to be instantaneous. In addition these authors suggest that as the granite layer cools it will grow in thickness and must therefore be crystallizing at the same time as melting is taking place at the roof which will have implications for the internal dynamics of the chamber during ascent (see section 5). Ascent and emplacement of these silicic magmas in the lower crust will be controlled by the same conditions as described previously.

Timing of the silicic magma generation has been modelled at 15, 30 and 45 Ma after thickening respectively (Fig. 5a). The thermal effects for this model of granite generation on the lithosphere are two fold. Firstly, the emplacement of the silicic magmas in the upper levels of the crust will have the same thermal and mechanical effect as in the model described above. Secondly, in addition to this process the pooling of the mafic magmas at and around the base of the crust will dramatically increase the thermal heat flux across the Moho and the potential for thermal weakening of the upper mantle (Fig 2a). Figure 5c shows that for all the critical times for magmatic emplacement much of the strength of the lithosphere is still concentrated in the

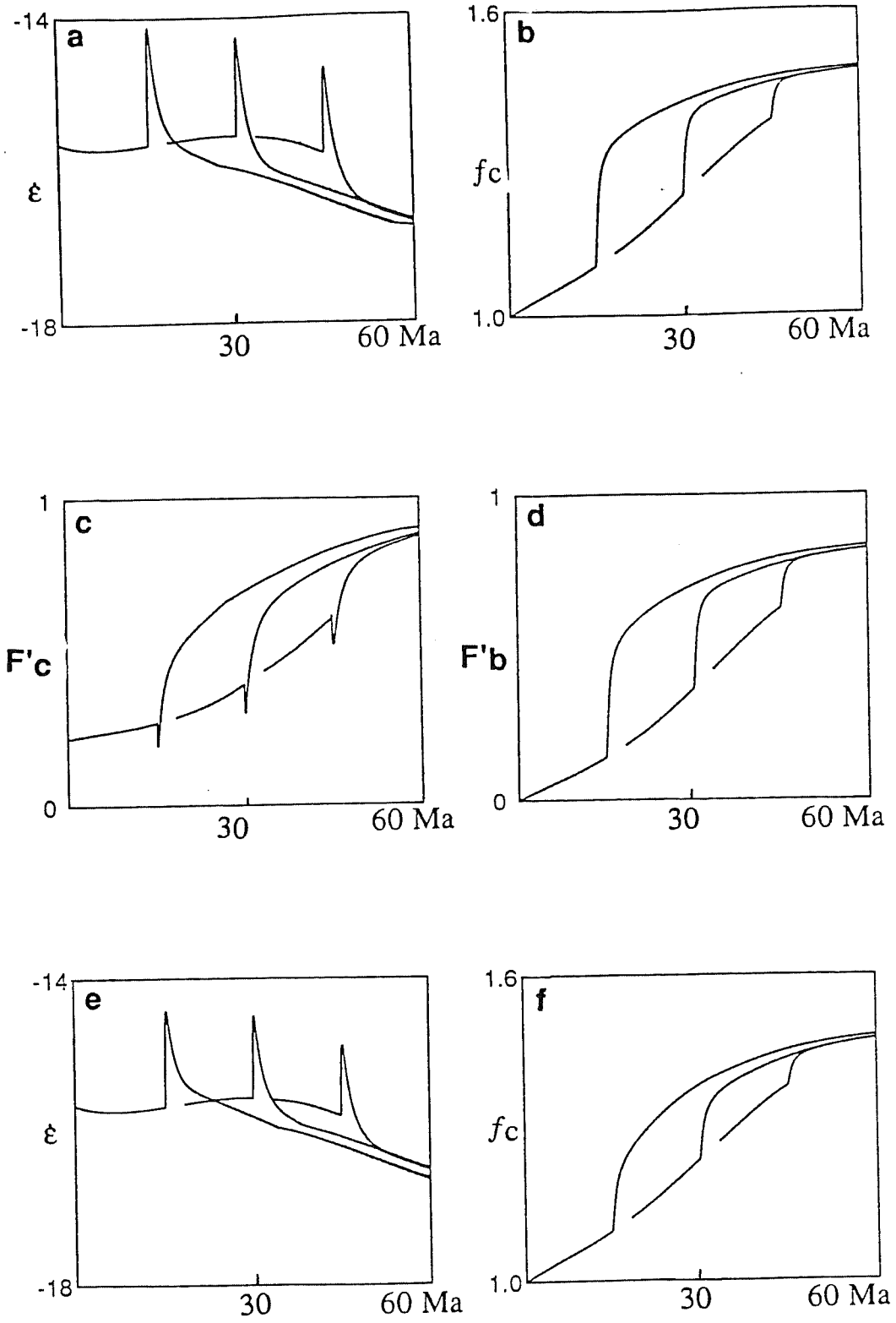

Figure 5

Plots for log strain rate, $\dot{\varepsilon}$, crustal thickening factor, f_c, buoyancy force on driving force, $F'_b = F_b/F_{dc}$ and crustal strength on lithospheric strength, $F'_c = F_{sc}/F_{sl}$, all against time for granitic generation via segregation from mafic magmas at the base of the crust. Granite generation is at an arbitrary 15, 30 and 45 Ma. Figures 5a-d correspond to strain model 2 with a driving force of 4×10^{12} Nm^{-1}, intrusion top at approximately 10 km with a granite thickness of 2.5 km. Figures 5e-f correspond to strain model 2 with a driving force of 4×10^{12} Nm^{-1}, intrusion top at 10 km with a granite thickness of 1.2 km.

upper mantle. Thermal weakening at both the lower and upper crust will rapidly thereby lower the strength of the lithosphere increasing the crustal strain and buoyant potential of the orogen (Eqn. 5). This process will allow significant crustal strain increments (Fig. 5b) with vertical strain rates above 10^{-15} s^{-1} for 5-6 Ma creating the potential for substantial regional deformation. However, even after significant crustal strain due to the advective heat, F_b will be too low for the limiting condition for the suspension of deformation (ie. $F_b = F_{dc}$) and deformation will continue beyond the time span for the thermal decay of the granite. The crust will continue to thicken after the thermal effects of the magma, but at a reducing rate until a level of 1.5 f_c is reached. This is attained after approximately 60 Ma. Figures 5a and 5b show the effect of silicic magma thickness on the deformation. Doubling the thickness of the silicic magma and consequentially the thickness of the mafic sill at the base of the crust will increase the thermal influx to the lithosphere allowing a marked increase in the crustal strain (figs. 5a, 5b).

3.1. Justification

Naturally the validity of such a model must be questioned as to its ability to successfully approximate the conditions in an orogenic event. It must be stressed here that this model is only an attempt to place constraints on the role of magmatic intrusion in the development of high temperature-low pressure metamorphic terrains rather than specific application to any one geological province. The fact that the model produces configurations analogous to observed situations, such as the approximate doubling of the crust observed in the Himalayan mountain chain, indicates that these models are capable of successfully constraining continental deformation.

4. A HIGH T-LOW P METAMORPHIC TERRAIN: AN EXAMPLE FROM PALMER, SOUTHERN ADELAIDE FOLD BELT.

4.1. INTRODUCTION

To augment the theoretical component of this thesis a field study was undertaken to examine the relationship between magmatic intrusion and deformation in the high T - low P 'Buchan style' metamorphic terrain (Sandiford *et al,* 1990) in the Palmer region of the South

Adelaide Fold Belt. The mapped region (Fig. 6) forms part of the highest metamorphic grade region of the Kanmantoo Group characterised by sillimanite facies metamorphism and migmatites which have been intruded into by the syn-tectonic orthogneissic Rathjen Gneiss and Palmer Granite. Structural analysis was conducted to evaluate this relationship between the Rathjen Gneiss and the surrounding metasediments and in the course of this investigation several new interpretations have been made on the nature and style of deformation in the highest grade rocks of the Kanmantoo Group.

The Kanmantoo Group forms the youngest sequence of the Southern Adelaide Fold Belt and consists of a thick sequence of non-fossiliferous, Cambrian 'flysch like' metasandstones and siltstones with interlayered marbles and calc-silicates (Milnes, 1982). This sequence was deposited in a rift like (Parkin, 1969) basin stretching from Kangaroo Island in the south to Eudunda in the north. During the Cambrian to Early Ordovician Delamerian Orogeny (Daily *et al*, 1976) the Southern Adelaide Fold Belt suffered significant deformation and metamorphism. Three major folding deformation phases have been recognised (Offler and Fleming, 1968, Mancktelow, 1979) with D_1 producing the dominant structural expression throughout the Fold Belt. However, significant overprinting by the D_2 crenulation event has occurred in the higher metamorphic grade regions. The third deformation is only local and non-pervasive. The metamorphism is high temperature - low pressure 'Buchan style' metamorphism (Sandiford *et al*, 1990) with distinctive increasing metamorphic zonation around the intrusive granitoids. Zones closest to the intrusives are characterised by migmatites and sillimanite facies metamorphism which grades to andalusite-sillimanite and finally biotite facies. Timing of the peak metamorphism in the Springton region based on microstructural evidence, such as inclusion trails in cordierite porphyroblasts, has been put as approximately coeval with the second deformation event (Mancktelow, 1979, Sandiford *et al*, 1990).

In the mapped region the Kanmantoo Group consists of three main metasedimentary units. The structurally lowest unit of the area is a hard, massive tremolite gneiss flanking the eastern margin of the mapped area. Structurally above the tremolite gneiss is a thick sequence of semi pelitic and psammitic migmatitic schists with primary sedimentary structures indicating that the sequence is the right way up. Interbedded with the above schists is a third unit

Figure 6

Key;

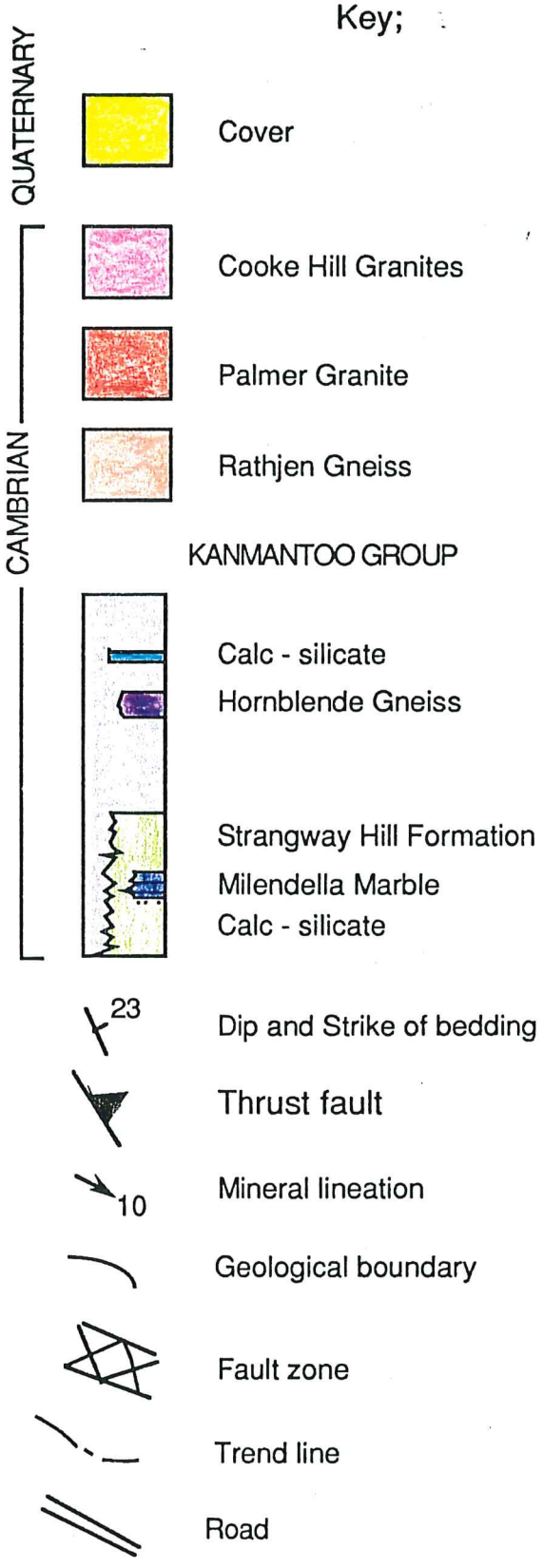
QUATERNARY
CAMBRIAN
Cover
Cooke Hill Granites
Palmer Granite
Rathjen Gneiss
KANMANTOO GROUP
Calc - silicate
Hornblende Gneiss
Strangway Hill Formation
Milendella Marble
Calc - silicate
23
Dip and Strike of bedding
Thrust fault
10
Mineral lineation
Geological boundary
Fault zone
Trend line
Road

Geology of the Palmer - Springton Region

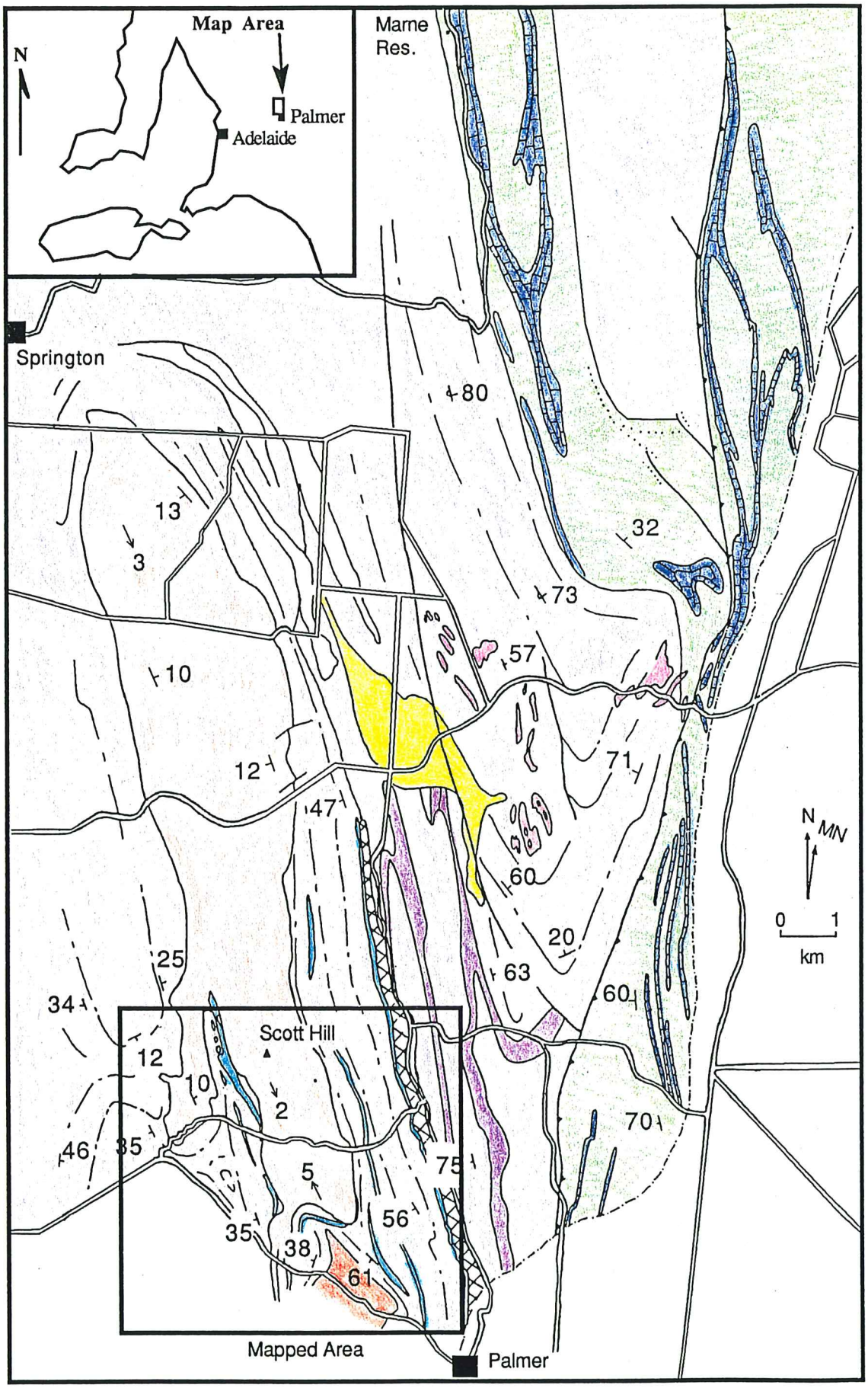

after Abbas (1975), Mills (1964) and Madigan, (1988)

alm	almandine
ann	annite
ap	apatite
bt	biotite
diop	diopside
fib	fibrous sillimanite
gnt	garnet
hnb	hornblende
kfsp	potassium feldspar
mu	muscovite
mag	magnetite
ph	phlogopite
plag	plagioclase
py	pyrope
ser	sericite
sph	sphene
q	quartz

Table 2

List of abbreviations used in text.

consisting of calc-silicates. These calc-silicates are up to 12 metres thick and composed of feldspar, quartz and hornblende with varying percentages of diopside and garnet. Three intrusive bodies can be recognised and are the Rathjen Gneiss, Palmer Granite and amphibolites. Geochemical investigations by Madigan (1988) and Foden (1990) have classified the Rathjen Gneiss and Palmer Granite as syn - tectonic intrusives with respective ages of 516 Ma and 490 Ma (Foden, in prep). Detailed description of the lithologies of the Palmer region are presented in appendix B.

4.2. STRUCTURE OF THE PALMER REGION

Two main phases of folding deformation can be recognised in the Palmer region with the second phase of deformation controlling the regional outcrop pattern. Due to the lack of mappable marker units, interpretation of the area is limited to structural overprinting criteria. Terminology that will be used has been defined as follows;

i) Two folding deformations D_1 and D_2 forming F1 and F_2 folds with associated S1 and S_2 fabrics respectively and an L_2 lineation.

ii) One brittle deformation D_3 forming major brittle faulting.

4.2.1. First Deformation (D_1) Folding

Although D_1 is the predominant structure of the lower grade regions of the Adelaide Fold Belt (Mancktelow, 1979) this first phase of folding has little expression in the mapped area due to the major overprinting of the D_2 folding event. F_1 folds form recumbent to reclined, tight to isoclinal, asymmetric similar style folds with moderate hinge thickening and limb attenuation (Plate 1a). Based on Ramsay's (1967) dip isogon classification the F_1 folds exhibit alternating layers of class 1c and 3 which together with limb shearing (Plate 1b), indicates thickening as a result of buckle folding with progressive development of shear flow in the limbs. Layers of high biotite content exhibit extreme shortening with the development of ptygmatic folding. S_1 is defined by the preferred orientation of mica and, in some cases, sillimanite which forms a pervasive layer parallel foliation.

Migmatitic melts found throughout the area exhibit a variety of structural relationships with overprinting relationships indicating both pre and post D_1 generation. The migmatites are generally layer parallel to $S_{0\text{-}1}$ with similar folding style to F_1 folds indicating pre or contemporaneous generation with the first phase of deformation (Plate 1c). Continued generation is implied with the development of cross-cutting layering, melt pods in necking zones of boudinage and axial planar melts indicating continued elevated temperatures well into the second deformation.

4.2.2. Second Deformation (D_2) Folding

F_2 is characterised by macroscopic open upright cylindrical folds with clear refolding of the S_1 fabric about the F_2 fold hinges without the development of any further axial planar fabric. Mesoscopic expression of this folding event is a non-pervasive crenulation of the D_1 fabrics and is particularly evident in the F_2 fold hinges. Stereographic analysis of bedding (S_1 parallel) indicates the F_2 fold axis plunging 15° towards 165° (Fig. 7). This crenulation folding noticeably increases in intensity further away from the Rathjen Gneiss culminating in an axial planar fabric, S_2 (see Fraser, 1990). Local development of a sub-vertical S_2 foliation is evident in a zone bordering the Palmer Granite. The mineral lineation, L_2, parallel to the F_2 fold axis, is a defined by the preferred orientation of mica in the metasediments and hornblende

aggregates in the amphibolites. A further manifestation of this north - south extension is seen in the development of boudinage structures in both the sedimentary layers and the migmatite melts. This boudinage has notably affected the calc-silicate layers resulting in extremely discontinuous out-crop along strike implying considerable extension accompanying S_2.

a) b)

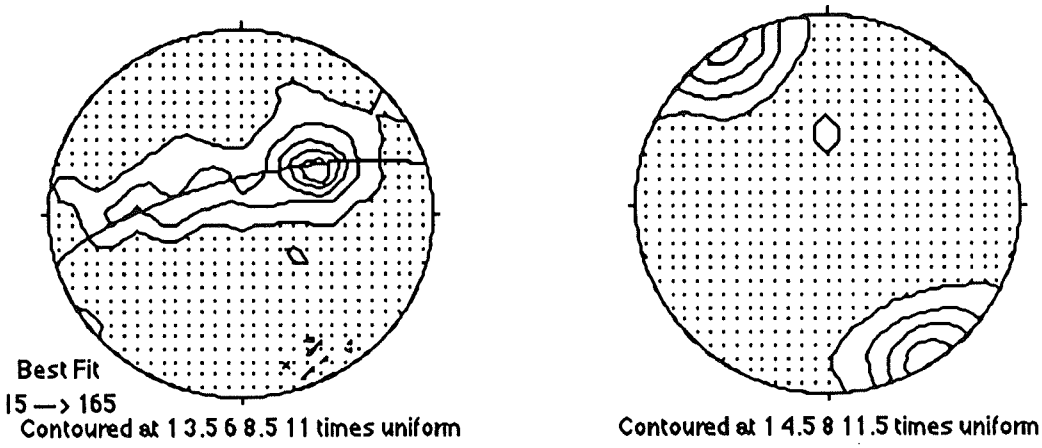

Figure 7

Steriographic plots for: a) F_2 bedding (S_1 parallel) with ♦ representing mesoscopic crenulation fold hinges and b) L_2 lineation

4.2.3. Third Deformation (D_3) Faulting

The D_3 is a late stage brittle faulting event which has produced a major breccia zone running parallel to the Palmer-Springton Road. The exposures are characterized by extensive vein filling of hematite and vuggie quartz indicating a period of extension during fluid infiltration. Talc rocks and intrusives mapped by Madigan (1988) suggests the fault extends for some distance further to the north. To the south, the mapped fault is the extension of the Tertiary Palmer Fault which bounds the present exposures of the Adelaide fold Belt. As the fault is sub-parallel to the regional bedding the degree of throw on the fault could not be determined.

In contrast to the work by Fleming and White (1984) I have found no evidence of further folding deformations in the area based on field observations and stereographic analysis.

Plate 1

1a Inclined F_1 with moderate hinge thickening and limb attenuation. Light coloured leucosomes exhibit general layer parallel orientation with some axial planar development (far left).

1b Close to tight F_1 folds with advanced limb shearing

1c Migmatitic schist displaying the layer parallel nature of the leucocratic melts. Scale 1cm

1d Contact between the Rathjen Gneiss and the Kanmantoo Group with laths of metasediment (near hammer handle) within the Gneiss. Outcrop of metasediment can be seen in the background of photo.

1e Polished cut of the mineral lineation within the Rathjen Gneiss defined by potassium feldspar, biotite and quartz ribbons. Scale 1cm.

a

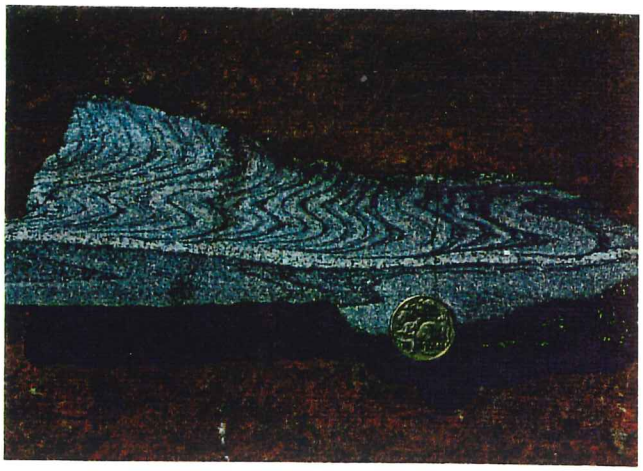

b

c

d

e

4.2.4. Granitic Intrusives

4.2.4.1. The Rathjen Gneiss

The nature and origin of the Rathjen Gneiss has been subject to a deal of controversy. Previous investigations by White (1966), Fleming and White (1984) and Fleming (1988) have argued that the Gneiss is an isochemically metamorphosed volcanic. However, decisive field and geochemical evidence put forward by Madigan (1988) indicates that the Gneiss is a syn-tectonic, I-type granitic intrusive with ion - microprobe dating revealing an age of 516 +/- 4 Ma. (Foden et al., in prep.). Due to the poor outcrop through the area, true contact relationships between the Rathjen Gneiss and the surrounding metasediments can be seen only at a few localities and in each case typical intrusive contacts can be observed (Plate 1d), supporting the interpretation of Madigan (1988). The continuity of the structure across the contact of the Gneiss is difficult to determine due to the poor quality of outcrop and the folding of the Gneiss by the D_2 event. The Gneiss forms a north-south striking elongated granitic body with a sub horizontal foliation and mineral lineation (appendix D, map A). This foliation is concordant with the boundary of the Gneiss and is defined by the preferred orientation of biotite aggregates. The foliation is generally non-pervasive due to the varying amounts of biotite. Sub-horizontal, the foliation dips generally less than 20° and forms an apparent synform with an axial plane parallel to F_2 folds experienced by the metasediment suggesting the Gneiss has suffered the D_2 folding event. The dominant mineral lineation is sub parallel to the F_2 fold axis and discordant with the northern and southern extremities of the Gneiss. Defined by the preferred orientation of potassium feldspar, quartz ribbons and biotite aggregates (Plate 1e) the lineation strikes NNW-SSE (Fig.8) but shows a systematic anti-clockwise rotation with respect to the southern extent of the Gneiss. Unlike the northern exposures of the Gneiss the plunge is not consistently to the south (Madigan, 1988) but rather double plunging to the north and south at angles less than 15°. Throughout the Gneiss there appears to be little variation in the intensity of the lineation. Both the foliation and lineation indicate that the Gneiss has undergone the second deformation event placing a lower age limit on the D_2 event. The occurrence of folded xenoliths within the Gneiss indicate intrusion either pre or syn - deformational synchronous with the D_1 event.

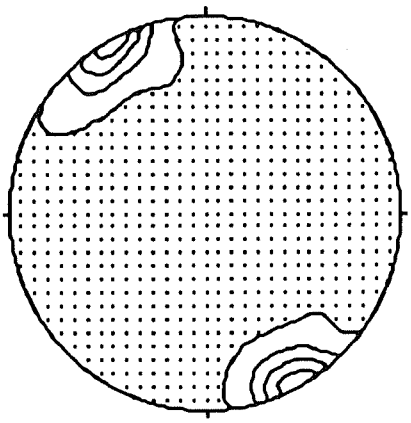

Figure 8.

Steriographic plot for the mineral lineation within the Rathjen Gneiss

Due to the lack of kinematic structures, detailed strain analysis is virtually impossible. However, in order to gain some appreciation, preliminary strain analysis on cobalti - nitrite stained alkali feldspars was conducted using the Flinn method (1962). Measurements on each XY (parallel to foliation, and lineation) and YZ (orthogonal to lineation and foliation) surface were taken in order to determine the configuration of the strain ellipsoid and in each case a mean reading was taken for the respective faces. The resultant shape factor K defined by Flinn (1962) is of the apparent constriction type resulting in a prolate strain ellipsoid with an intensity factor of 4 (Watterson, 1968).

4.2.4.2. Palmer Granite

The Palmer Granite is located approximately 2 km to the east of Palmer and is oval shaped in out-crop. The surrounding metasediments show clear warping around the Palmer Granite and the development of a sub vertical foliation indicating its syn-tectonic emplacement. The intrusion of the Palmer Granite has not only affected the surrounding country rock but also the Rathjen Gneiss causing the rotation of the lineation in the southern reaches of the Rathjen Gneiss. In contrast to the highly deformed Rathjen Gneiss, the Palmer Granite exhibits virtually no internal deformation. This is probably due to two factors i) its late intrusion into the deforming sequence and ii) its predominant feldspar mineralogy. Vernon and Flood (1988) indicate that granitic bodies consisting of predominantly plagioclase show little or no internal

deformation due to the relative strength of plagioclase over the more ductile minerals such as the quartz and potassium feldspar which dominates the Rathjen Gneiss.

4.2.4.3 Amphibolites

The amphibolites of the area are, in general, layer parallel to the regional bedding. As a result of boudinage the amphibolites are extremely discontinuous along strike and display characteristic intrusive relationships indicating either pre or syn - deformation. Internal structural features are limited to a dominant mineral lineation defined by the preferred orientation of hornblende aggregates.

4.3. METAMORPHISM

4.3.1. Metamorphic Relationships

In this section the relationships between the timing of mineral growth and deformation will be demonstrated via microstructural evidence. The principal mineral assemblages for the metasediments in the mapped area are given in Table 3.

The peak metamorphic assemblages in the metasediments are characterised by qtz + kfsp + plag + bt +/- sil and gnt with minor sphene, apatite and magnetite. Indications that this prograde metamorphism occurred during deformation are the distinctive deformation lamellae in both plagioclase and potassium feldspars with quartz exhibiting undulose extinction. The timing of this metamorphism can be constrained by the relationships of mineral growth to the deformation fabrics. Forming the predominant S_1 fabric through the area is the preferential alignment of biotite and, in areas, fibrous sillimanite. Plate 2a shows that, while the fibrous sillimanite may be considered a part of the prograde mineralisation, preferred crystallisation at the grain boundaries of potassium feldspar indicates growth after the setting of the peak metamorphic grain boundaries. The fibrolite forms distinctive radiating pods on the S_1 foliation plane (Plate 2b). The lack of prograde andalusite and reaction textures with the micas indicates that the production of the fibrolite is via de-alkilisation of potassium feldspar. This microstructural evidence indicates that the fibrolite was formed late in the development of the D_1 deformation suggesting continued elevated temperatures.

	934-14	934-36	934-39	934-43	934-45	934-101
apat	P		P		P	
bt		Pf				Pf
diop	Ppl					
fib		Pf				
gnt			P			P
hnb	Ppl		P	Pl	Pp	
kfsp	P	Pm	Pm		Pm	P
mag			P		P	
mu		R				
plag	P	P	P	Pl		P
ser		R		R		
sph	P		P		P	P
q		P			P	P

Table 3

Selected mineral assemblages for the predominant lithologies within the mapped area where P is Prograde, R is retrograde and P is porphyroblastic. Syn-tectonic foliation and lineation are represented by f and l respectively.

These elevated temperatures are not unexpected as shown above the migmatite melts persisted through the deformation and continued to the D_2 event indicating temperatures in excess of 650°C. Further evidence for syn-tectonic prograde mineralisation is the porphyroblastic growth of skeletal garnet in the psammitic schists and hornblende in the calc-silicates. Shown in plate 2c is the wrapping of the biotite fabric around the garnets. The skeletal growth of the porphyroblasts indicates reasonably rapid growth.

Mineral associations with the development of the second deformation are restricted to the crenulation of the biotite and fibrolite fabrics and the oriented growth of mica and hornblende aggregates forming the L_2 lineation (Plate 2d) without the development of any further mineral growth. This is contrary to the areas of lower grade metamorphism where the peak metamorphic growth was during or following the second phase of deformation based on inclusion trails in cordierite (Mancktelow, 1979, Sandiford *et al*, 1990). This suggests that the peak metamorphism is not only spatially distributed but also time dependent with the timing of peak metamorphic temperatures increasing with distance away from the Rathjen Gneiss.

Retrograde reactions have been restricted to the breakdown of fibrolite and sericitisation of plagioclase. Plates 2b and 2e displays the retrograde muscovite coronas around

the fibrolite with figure 2g showing the break down relationship of both fibrolite and potassium feldspar to muscovite. Muscovite mineralisation exhibits no deformation suggesting that the retrograde mineral growth post dates all deformation events.

4.3.2. Physical Conditions

The pressure temperature conditions of the Springton region (Fig. 6) have been calculated by Arnold (1989) and Sandiford *et al* (1990) using the data set of Holland and Powell (1985). They established temperatures of 530-680°C at 3-5 kbars with essentially isobaric prograde metamorphism interpretated from progressive replacement of early kyanite by andalusite and then fibrous sillimanite in quartz segregations from the Marne Reserve (Fig.6: Sandiford *et al* , 1990). In the mapped region temperatures of 603-691°C were obtained at pressures of 3-5 kbars from gt+bt+plag+kfsp schist. To substantiate these results pressure-temperature estimates using geothermometer calibrations of Ferry and Spear (1978) and Hodges and Spear (1982) were used in this study. These calibrations are based on the partitioning of iron and magnesium between alm py ann and ph base on synthetic mineral assemblages (Ferry and Spear, 1978) which have been corrected for natural mineral assemblages (Hodges and Spear, 1982). Results from the calibrations reveal slightly higher temperatures of 712°C (Ferry and Spear,1978) and 720°C (Hodges and Spear, 1982)at 5 kbars.

In summary, the peak metamorphic conditions experienced by the Palmer area occurred during the concluding stages of the first deformation at temperatures of 603°-691°C and pressures of 3-5 kbars. Together with local partial melting of the metasediments indicates that peak local temperatures were experienced at the time of intrusion of the Rathjen Gneiss.

5. DISCUSSION

The development of the high T - low P terrain in the Palmer region has shown a decided relationship between advective heat, peak metamorphism and deformation. Field constraints on the total strain experienced by the area are too difficult to otain and thus comparison with the numerical model is required in order to gain some appreciation for the processes that have occured. In order to produce the significant D_2 event in the Palmer region associated with the intrusion of the Rathjen Gneiss a process analogous to the second model is

Plate 2

2a Fibrolite growth at the grain boundaries of potassium feldspar. Field of view 2mm

2b S_1 fibrolitic fabric with retrograde corona of muscovite. Field of view 2mm

2c Porphyroblastic garnet with biotite fabric. Field of view 2mm

2d L_2 lineation defined by the preferred orientation of amphibole aggregates. Field of view 2mm

2e Retrograde muscovite reacting with fibrolite and potassium feldspar. Field of view 2mm

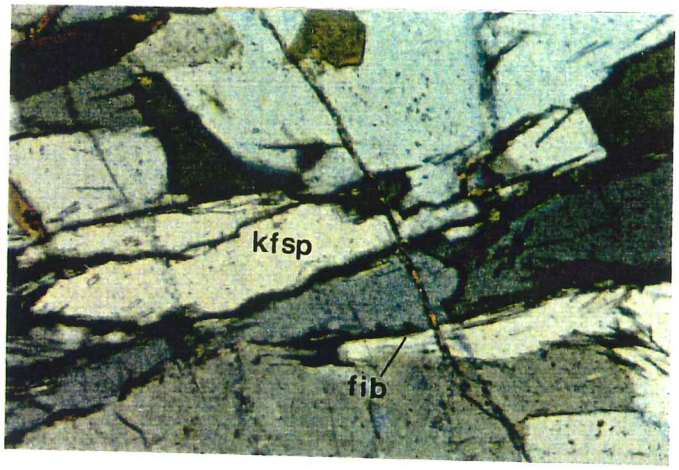

a

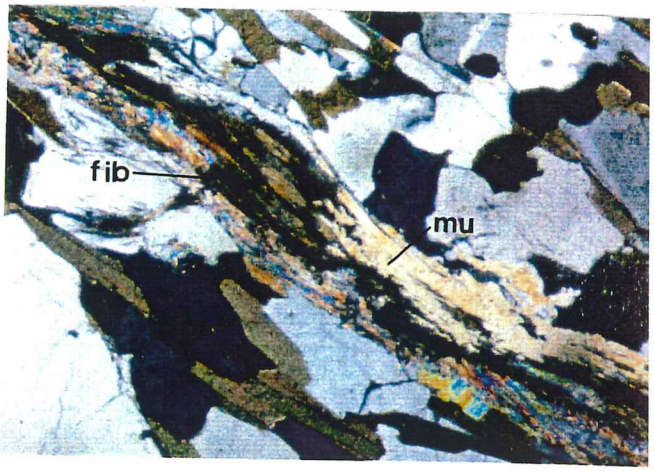

b

c

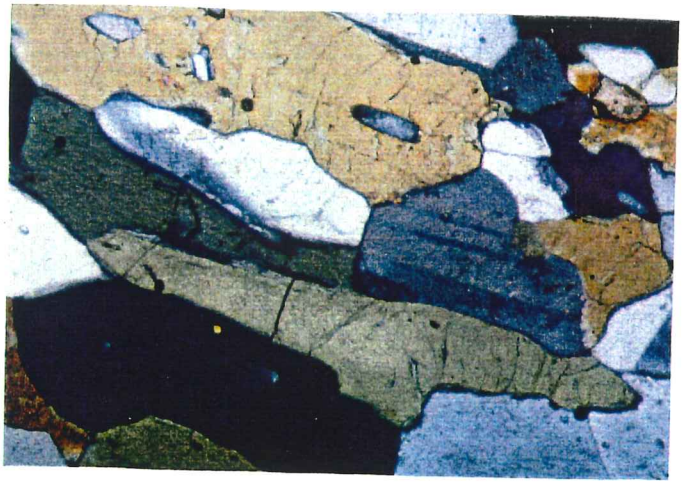

d

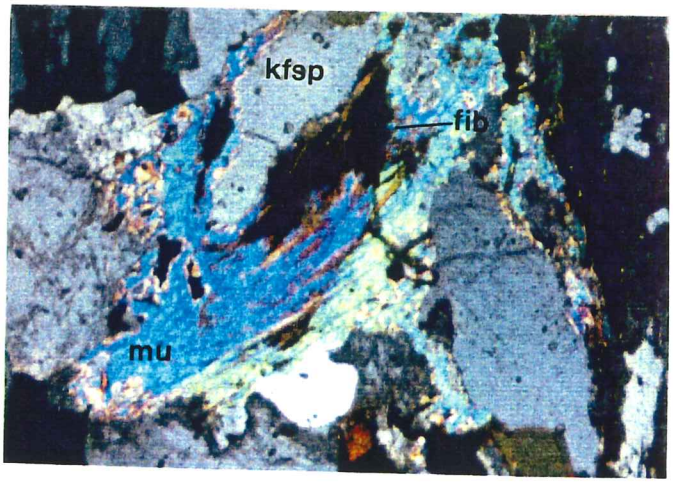

e

required. It is unlikely that silicic magma generation due to lower crustal melting could cause the observed effects due firstly to the early intrusion of the Rathjen Gneiss. Recent geochemical data (Cooper *et al*, 1990) indicates the deposition of the basal units of the Kanmantoo Group approximately 10 Ma prior to the intrusion of the Rathjen Gneiss. In order to produce such an effect unrealistic initial configurations would be required. In addition to this it has been shown that the scale of the crustal thickening produced by such a model will be too small to produce the significant local D_2 deformation. Initial compressive deformation of the Kanmantoo Trough produced the D_1 folding deformation. Intrusion of the the orthogneissic Rathjen Gneiss would have caused local temperature elevation, partial melting and peak prograde metamorphism. The thermal perturbation will rapidly lower the strength of the crust and in turn increase the buoyancy force. This process will result in a rapid increase in the crustal strain increments with strain rates in the order of 10^{-14} s^{-1} and the production of the substantial D_2 folding deformation with an axial planar fabric S_2. During the ascent of the Rathjen Gneiss the buoyancy contrasts will result in significant vertical compression in excess of the sub-horizontal compression, causing crustal thickening, resulting in a local vertical principal compressive stress. Modelling by Huppert and Sparks (1988) suggests that crystallization of the granite will occur during formation and thus these aggregates will be subjected to the local strain forming a sub-horizontal foliation. The surrounding country rock will also be affected by the buoyant rise of the granite with local rotation or generation of sub horizontal structural fabrics. The vertical compression and local high temperatures will effectively shield the surrounding country rock from the second generation deformation which becomes progressively stronger further away from the Gneiss. Extension of the Gneiss will occur in the third strain axis perpendicular to the vertical and horizontal compressive stresses either during or post-dating ascent resulting in a prolate strain ellipsoid. This extension is shown by the growth of potassium feldspar in the pressure shadows of relic phenocrysts of plagioclase. Modelling of the thermal decay from a magma (see Fraser 1990) reveals that with increasing distance away from the intrusion the peak metamorphic temperature will occur at increasingly later stages. Consequently at the time of intrusion of the Rathjen Gneiss (time a, Fig.9) the areas immediately adjacent will experience peak metamorphic temperatures, with

mineral growth, such as the fibrous sillimanite, dictated by the first deformation. Areas at some distance from the Gneiss will experience peak temperatures at some time after intrusion (time b, Fig.9) with mineral growth governed by the D_2 event producing microstructural features such as curved inclusion trails in cordierite assemblages (Sandiford *et al*, 1990). Derivation of the Gneiss and the Palmer Granite from a lower crustal mafic sill is backed up by the geochemical evidence discussed by Foden *et al* (1990) on the Delamerian magmatism in the Southern Adelaide Fold Belt. Their results indicate that the the syn-tectonic magmas consist of a large primitive component suggesting derivation from a mafic source. As indicated by Foden et al (1990) the likely source for these mafic magmas is underplating during the extended periods of rifting during the deposition of the Adelaide Fold Belt and in particular the rifting of the Kanmantoo Trough.

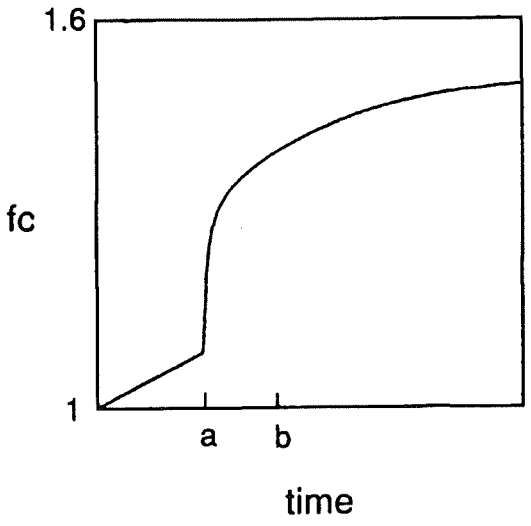

Figure 9

At time a, peak metamorphic temperatures will be experienced at the time of intrusion, and with little crustal thickening strain associated with the second deformation at this time mineral growth will be subject to the first deformation. At some distance from the intrusion peak metamorphic temperatures will occur at time b, and as significant crustal strain associated with the D_2 event has occurred, mineral growth will be subject to this second deformation.

ACKNOWLEDGMENTS

First and foremost my sincere thanks to my supervisor, Mike Sandiford for his continued enthusiasm, patience and willingness to help throughout the year.

Many thanks are also extended to Kurt Stüwe, Peter Dymoke, Simon Turner, John Foden and Pat James for their helpful comments and discussions throughout the year.

Thanks to the technical staff of the Department of Geology in particular Wayne Mussared and Geoff Trevelyan. Hugh Rosser at the University of Adelaide Electron Optical Centre is thanked for his patience and assistance on the microprobe.

To the other honours students and in particular Barry and Geoff for their continued source of enjoyment and amazement through the last year. Thanks to Dean and Donna and the land owners at Cambrai for their warm hospitality.

To my family and friends, especially my parents, for their support and encouragement over the last four years and finally Fiona for her continued support.

References

Abbas, S.A.F., 1975, Granitic and migmatitic rocks of the Cooke Hill area, South Australia, and their structural setting. Ph.D thesis, University of Adelaide (unpubl.)

Arnold, J., 1989, Petrogenesis of Cordierite - Orthoamphibole rocks from the Springton region, Mt Lofty Ranges. Hons. Thesis, University of Adelaide (unpubl.).

Brace, W.F and Kohlstedt, D.L., 1980, Limits on Lithospheric Stress Imposed by Laboratory Experiments., *J. Geophy. Res.*, **85**, 6248-6252.

Byrlee, J.D., 1968, Brittle and ductile transition in rocks., *J. Geophy. Res.*, **73**, 4741-4750.

Cooper, J.A., Jenkins, R.F.J., Compston, W. and Williams, I.S., 1990, Ion microprobe U-Pb zircon dating within the lower Cambrian of South Australia. *Geol. Soc Aust. Conf. Abstracts.*, **No 27**, pp 21

Daily, B., Firman, J.B., Forbes, B.G. and Lindsay, J.M., 1976, Geology. *In* Twidale C.R., Tyler, M.J. and Webb, B.P., eds. Natural History of the Adelaide Region. *R. Soc. S. Aust.*

England, P.C. and Houseman, G.A., 1988, The mechanics of the Tibetan Plateau, *Phil.Trans.R.Soc.Lond.*, **326**, 301 - 321.

England, P.C., and Thompson, A.B., 1984, Pressure - temperature - time paths of regional Metamorphosm 1. Heat transfer during the evolution of regions of thickened continental crust, *J.Petrol.*, **25**, 894 - 928.

Ferry, J.M. and Spear, F.S., 1978, Experimental calibration of the partitioning of Fe and Mg between biotite and garnet. *Contirb Mineral Petrol*, **66**, 113-117

Fleming, P.D., 1988, South of Scott Hill - Rathjen Gneiss. *In* Gatehouse, C.G. (compiler), Kanmantoo Field Symposium Excursion Guide., Rept. Bk. No. 88/35. S.A.D.M.E.

Fleming, P.D., and White, A.J.R., 1984, Relationships between deformation and partial melting in the Palmer migmatites, South Australia., *Aust. J. Earth Sci.*,**31**, 351-360.

Flinn, D., 1962, On folding during three dimensional progressive deformation, *Quartterly J. Geol. Soc Lond*, **118**, 385-433.

Fraser, G.L., 1990, High T - Low P metamorphism in the Kanappa Hill Area of the Mt Lofty Ranges; implications for the thermal evolution of the terrain. Hons.thesis, University of Adelaide (unpubl.).

Foden, J.D., Williams, I., Compston. W., Michard, A. and Turner, S.P., in prep, The timing and Duration of the Delamerian Orogeny.

Gans, P.B. and Miller,E.L, 1989, Cretaceous crustal structure and metamorphism in the hinterland of the Sevier thrust belt, western U.S. Cordillera., *Geology*, **17**, 59-62.

Goetze, C., 1978, The mechanism of creep in olivine., *Phil. Trans. R. Soc. Lond.*, **288**, 99-119.

Hodges, K.V. and Spear, F.S., 1982, Geothermometry, geobarometry and the Al_2SiO_5 triple point at Mt. Moosilauke, New Hampshire. *Amer. Mineral.*, **67**, 1118-1134.

Holland, T.J.B. and Powell, R., 1985, An internally consistant thermodynamic data set with uncertainties and corrections: 2 Data and results. *J Met. Geol.*, **3**, 343-370

Houseman, G.A., McKenzie, D.and Molnar, P., 1981, Convective instability of a thickened boundary layer and its relevence for the thermal evolution of continental convergent belts. *J. Geophy. Res*, **86**, 257-267.

Huppert, H.E and Sparks, S.J., 1988, The fluid dynamics of crustal melting by injection of basaltic sills., *Trans. R Soc Edinburgh.*, **79**, 237-243.

Loosveld, R.J.H., 1989, The synchronism of crustal thickening and high T/ low P metamorphism in the Mount Isa inlier, Australia. part II: fast convective thinning of mantle lithosphere during crustal thickening. *Tectonophysics*. in press.

Loosveld, R.J.H., and Etheridge, M.A., 1990, A model for low - pressure facies metamorphism during crustal thickening, *J.Metamorph.Geol.*, **8**, 257 - 267.

Madigan, T.L.A., 1988, Constraints on the tectonic history of the Kanmantoo group around Springton, South Australia. Hons. Thesis, University of Adelaide (unpubl.).

Mancketelow, N.S., 1979, The Structure and Metamorphism of the Southern Adelaide Fold Belt., Ph.D. Thesis. University of Adelaide (unpubl.).

Mills, K.J., 1964, The structural geology of an area east of Springton, South Australia, Ph.D thesis, University of Adelaide (unpubl.).

Milnes, A.R., 1982, The Encounter Bay Granites and their relationship to the Kanmantoo Group. In Oliver, R.L.and Gatehouse, C.G. eds. *Guide to Excursions B1, B2, B3, B4, Geology of the Adelaide Region*: Fourth International Symposium on Antartic Earth Sciences.

Offler, R. and Flemming, P. D., 1968, A Synthesis of folding and metamorphism in the Mt. Lofty Rangers, South Australia, *J. Geol. Soc. Aust*, **15(2)**, 245-266.

Parkin, L. W., 1969, ed. *Handbook of South Australian Geology. Geol.* Sur. S. Aust.

Patterson, M.S., 1987, Problems in extrapolation of laboratory rheological data., *Tectonophysics*, **133**, 33-43

Ramsey, J.G., 1967, *Folding and Fracturing of Rocks*. McGraw-Hill Inc, New York. pp568

Sandiford, M., 1989, Secular trends in the thermal evolution of metamorphic terrains, *Earth.Plan.Sci.Lett.*, **95**, 85 - 96.

Sandiford, M., Oliver, R.L., Mills, K.J. and Allen, R.V., 1990, A cordierite - staurolite - muscovite - association, east of Springton, Mt. Lofty Ranges; Implications for the metamorphic evolution of the Kanmantoo Group. In Jago, J.B. and Moore, P.S. (eds). The Evolution of a late Precambrian - early Paleozoic rift complex: the Adelaide Geosyncline. Geol. Soc Aust. Spec Publ. No 16, 483 - 495.

Sandiford, M., and Powell, R., 1990, Some isostatic and thermal consequences of vertical strain geometry in convergent orogens, *Earth Plan. Sci. Lett.*, **98**, 154-165.

Sandiford, M.and Powell, R., in press, Isostatic and thermal constraints on the evolution of high temperature - low pressure metamorphic terranes in convergent orogens, *Earth.Plan. Sci.Lett.*

Shelton, G.and Tullis,J., 1981, Experimental Flow Laws for Crustal Rocks, *EOS,* **62(17)**, 396

Turcotte, D.L.and Schubert, G., 1982, *Geodynamics: applications of continuum physics to geological problems,* Wiley, New York.

Vernon, R. H.and Flood, R.H., 1988, Contrasting deformation of S- and I- type granitoids in the Lachlan Fold Belt, eastern Australia., *Tectonophysics.*, **147**, 127-143.

Watterson, J., 1968, Homogeneous deformation of the gneisses of Vesterland, South - West Greenland. *Medd. Gronland.*, **175**, 6

White, A.J.R., 1966, Petrology and Structure of the Rathjen Granitic Gneiss of the Palmer Region, South Australia., *J. Geol. Soc. Aust.*, **13(2)**, 471-489.

APPENDIX A :

a) Geothermal Gradient:

The initial geothermal gradient defines the initial thermal distribution of the lithosphere. The derivation described here follows closely that described by Turcotte and Schurbert, 1982

Conductive heat transport through a medium of differing temperatures is described by Fourier's law and takes the form:

$$q = - k \frac{\partial T}{\partial z}$$

where q is heat flow, $(\partial T/\partial z)$ is the temperature gradient in the medium and k is conductivity. For one dimension the change in thermal structure of a body by heat conduction is equal to the gradient of the heat flow across the body multiplied bt the thickness of the body. In the steady state, ie no change in temperature with time, this will equal zero. Thus:

$$0 = \partial z \frac{\partial q}{\partial z}$$

$$= \partial z \ - K \frac{\partial^2 T}{\partial z^2}$$

The heat production per unit volume is given by:

$$\rho \, H \, \partial z$$

where r is the density and H is the volumetric heat production.

By equating the above terms the thermal energy balance can be expressed:

$$0 = K \frac{\partial^2 T}{\partial z^2} + \rho \, H$$

For appropriate boundary conditions for the continental lithosphere of:

$$q = qs \quad \text{and} \quad T = Ts \quad \text{at} \quad z = 0$$

where qs is the surface heat flow and Ts is the surface temperature integration of the above equation gives the temperature, Tz, at any depth:

$$Tz = Ts + \frac{q_s z}{k} - \frac{\rho H z^2}{2 k}$$

assuming constant heat source distribution.

b) Buoyancy Force:

The buoyancy force uses the formulation developed by Sandiford and Powell (in press). The buoyancy force per unit length, F_b, is given by the difference between the double integrals of density, both with respect to z, from the Earth's surface down to a common depth beneath the lithosphere, for the deformed and undeformed lithosphere respectively:

$$F_b = \int_{zl}^{h_o} \sigma_{zzo}(z)\, dz - \int_{z_l}^{h_o+h} \sigma_{zzd}(z)\, dz$$

where s_{zz} is the vertical stress and h_o and h are the initial elevations and deformed elevations respectively. Recasting in terms of crustal thickening factor, f_c and lithospheric thickening factor, f_l gives:

$$\frac{F_b}{\rho\, z\, c^2} = g\, d\frac{1-d}{2}(f_c^2 - 1) - \frac{aT_l}{6y^2}[f_l^2 - 1 - 3\,d\,(f_c f_l - 1)] - \frac{a^2 T_l^2}{8y^2}(f_l^2 - 1)$$

correct to second order in the 'small' terms d and aT_l, where T_l is the temperature at the base of the lithosphere, y is the ratio of crust to lithosphere and z_c is the depth to the Moho.

APPENDIX B :

In the mapped area three major lithologies namely the tremolite gneiss, psammitic metasediments and calc-silicates. These have been subsequently intruded by the Rathjen Gneiss, Palmer Granite and amphibolite dykes. All the mapped lithologies are within the highest grade, sillimanite facies, rock of the Kanmantoo.

Tremolite Gneiss

Structurally the lowest unit, the tremolite gneiss flanks the eastern extent of the mapped area forming a predominate N-S running ridge. The gneiss is a hard, massive, homogeneous quartz (90%), feldspar (8%) and tremolite(2%). Irregular grain boundries are common with undulose quartz and deformation lamell in plagioclase. In outcrop the gneiss shows little mineralogical variation and a weak n-s trending lineation defined by the preferred orientation of tremolite.

Metasediments

Forming the dominant lithology of the region is a thick sequence of high grade psammitic metasediments grading to migmatites near the Rathjen Gneiss. Direct contact to the underlying tremolite gneiss could not be observed but is suggested to be conformable. Mineralogically the metasediments consist of quartz, feldspar, biotite, muscovite +/- fibrolite and garnet with minor sphene and magnatite and show a deal of variation through the area as a result of their original composition. Feldspars exhibit common microcline twinning and perthitic textures. In outcrop this variation is expressed as finely bedded layers and the progressive increase in metamorphic grade to migmatites near the Rathjen Gneiss boundary. Petrography of the metasediments reveal fine grain size (<1.5mm) with low to mild intergranular equlibration based on grain boundary association. Fabrics developed are defined by the preferential alignment of biotite grains and, in some instances, fibrolitic growth of sillimanite.

Lower grade metasediments exhibit well bedded (10-20 cm thick) psammitic layers with primary sedimentary features such as cross bedding and flame structures rarely observable. All facing indicates the sequence is the wright way up and younging to the south west. Increasing grade to biotite schists and subsequently migmatitic melts, S_1 becomes more pronounced resulting in distinctive tor like outcrops. Migmatitic melts comprise of dominantly plagioclase with minor alkali feldspar and quartz and are bounded by a sleeve of biotite. Detailed geochemical analysis of these melts have been done by Fleming and White (1984) and Madigan(1988) concluding that they are the partially melted equivalent of the metasediment.

Calc-silicates

Interlayered with in the psammitic metasediments is a series of calc-silicate layers. The calc-silicates are notably discontinuous along strike and up to 12 metres thick. Mineralogically the calc-silicates comprise of feldspar (60-80%), quartz (10-20%), hornblende (1-10%) sphene (1-5%) +/- porphyroblastic growth of garnet (0-2%) or diopside (0-2%) with sporadic triple junctions indicating a degree of grain equlibration. As a result of their friable nature the calc-silicates are in general poorly out-cropping. Fabrics are restricted to composition layering as seen in sample 934-39 with garnet-hornblende risch and poor layers. Feldspars have undergone sericitisation with replacement of the calcic portions of the feldspars.

Rathjen Gneiss

The Rathjen Gneiss forms an north south elongate I-type syntectonic granitic body (Madigan, 1989). Mineralogically the Gneiss composes of quartz (30%), potassium feldspar (35%), plagioclase (25%) and biotite (10%) with minor magnatite, zircon mymercite and hornblende. Plagioclase occurs as relic undeformed phenocrystists with seritisation of the more calcic zones. Growing in the pressure shadows of the plagioclase are potassium feldspars which are commonly exhibit microcline twinning and perthitic textures. Quartz forms distintive ribbons with regrowth indicated by irregular grain boundries and undulose extintion. Biotite defines the sub-horizontal foliation withinb the Rathjen Gneiss. There is little compositional variation throughout the Gneiss.

Palmer Granite

The Palmer Granite forms an oval oval shaped body with and is predominately plagioclase feldspar with minor quartz.

Amphibolites

Amphibolite dykes can be seen through the area and are highly discontinuous.and although mainly concordant with the surrounding the Amphibolites display in sections typical discordant intrusive boundaries. Their mineralogy is predominantly hornblende (60%),

plagioclase (40%) and sphene (1%). A marked lineation fabric is defined by the preferred orientation of the amphibole grains.

LOCALITY MAP